POLITECNICO DI TORINO
Repository ISTITUZIONALE

A lattice Boltzmann formulation to the analysis of radiative heat transfer problems in a participating medium

(Article begins on next page)

17 May 2024

A LATTICE BOLTZMANN FORMULATION
TO THE ANALYSIS OF RADIATIVE HEAT TRANSFER
PROBLEMS IN A PARTICIPATING MEDIUM

Pietro Asinari*, Subhash C. Mishra** and Romano Borchiellini*

*Department of Energetics
Politecnico di Torino
Turin - 10129, Italy

**Department of Mechanical Engineering
Indian Institute of Technology Guwahati
Guwahati – 781039, India

Correspondence
Dr. Subhash C. Mishra
Professor
Department of Mechanical Engineering
IIT Guwahati
Guwahati – 781039, India
Email: scm_iitg@yahoo.com

Tel: 0091-361-2582660
Fax: 0091-361-2690762

Abstract

Usage of the lattice Boltzmann method (LBM) has been extended to analyze radiative transport problems in an absorbing, emitting and scattering medium. In terms of collision and streaming, the present approach of the LBM for radiative heat transfer is similar to those being used in fluid dynamics and heat transfer for the analyses of conduction and convection problems. However, to mitigate the effect of the isotropy in the polar direction, in the present LBM approach lattices with more number of directions than those being used for the 2-D system have been employed. The LBM formulation has been validated by solving benchmark radiative equilibrium problems in 1-D and 2-D Cartesian geometry. Temperature and heat flux distributions have been obtained for a wide range of the extinction coefficients.   The LBM results have been compared against the results obtained from the finite volume method (FVM). A good comparison has been obtained. The numbers of iterations and CPU times of the LBM and the FVM have also been compared. The number of iterations in the LBM has been found to be much more than the FVM. However, computationally the LBM has been found to be much faster than the FVM.

Nomenclature

a - anisotropy factor

c - speed of light

$\vec{e}_i$ - velocity in the discrete direction i

G - incident radiation

I - intensity

I_b - blackbody intensity, $\dfrac{\sigma T^4}{\pi}$

M - number of discrete directions

p - scattering phase function

q - heat flux

S - source term

s - geometric distance

T - temperature

t - time

U - speed

w - weight

X, Y - $x-$ and $y-$dimensions of the 2-D rectangular enclosure

x, y - $x-$ and $y-$coordinate directions

Greek Symbols

β - extinction coefficient

κ_a - absorption coefficient

ε - energy shell constant

γ - polar angle

δ - azimuthal angle

σ - Stefan-Boltzmann constant $= 5.67 \times 10^{-8} \, \text{W/m}^2.\text{K}^4$

σ_s - scattering coefficient

τ - relaxation time

Φ - dimensionless emissive power

Ω - direction, (γ, δ)

$\Delta\Omega$ - solid angle, $\sin\gamma \, d\gamma \, d\delta$

ω - scattering albedo $\left(\dfrac{\sigma_s}{\beta}\right)$

Ψ - dimensionless heat flux

Subscripts

b - black

E, W, N, S - east, west, north, south

i - index for the discrete direction

P - cell center

w - wall/boundary

x - x-boundary

y - y-boundary

Superscript

(eq) - equilibrium

1. Introduction

Consideration of volumetric radiation is important in many high temperature thermal devices and processes [1, 2]. Design of boilers, furnaces, internal combustion engines and insulations are some of the systems which require a correct analysis of thermal radiation [1, 2]. Analysis of phase change process of semitransparent materials such as glass and semiconductor materials requires knowledge of the volumetric radiation [3-6]. Correct estimates of volumetric radiation is also important in weather forecasting which relies on atmospheric radiation budget [7] and medium characterization of an optically participating medium like human tissue and laser surgery of a human organ [8-9].

Radiative transport through a participating medium is a volumetric phenomenon [10, 11]. Unlike conduction and convection modes of heat transfer which depends on spatial and temporal dimensions, an analysis of radiation involves an additional three dimensions, viz., two angular dimensions (polar and azimuthal angles) and one spectral dimension. A mandatory consideration of two angular dimensions in all problems except the simplest case of the planar geometry in which case radiation is azimuthally symmetric and thus it depends only on the planar angle, the problems are difficult to analyze. In a conduction-convection and radiation problem, it is the computation of radiative component that is the most time consuming. This excessive computational time in the computation of radiative information is for the reason that apart from covering all the spatial grid points in the solution domain, intensities at every grid point need to be traced from their points of origin in the enclosure to the grid point under consideration. At every grid point, intensities are spanned over the 4π spherical space. A method becomes computationally more expensive if for a given number of control volumes, it requires more number of discrete directions.

The available numerical radiative transfer methods such as the flux method [10,11], the zonal method [10,11], the spherical harmonics method [10,11], the discrete ordinates method (DOM) [12,13], the discrete transfer method (DTM) [14-16], the collapsed dimension method [17] and the finite volume method (FVM) [18-20], in some form or the other, aim at minimizing the angular dependency of radiation in their formulations. Since the angular dependency can not be fully eliminated, a method which is less prone to ray effect and is compatible to other CFD solvers such as the finite difference method (FDM) and the FVM for solving the combined mode problems in simple to complex geometry are the most desirable ones. Among the existing numerical radiative transfer methods, the FVM [18-20] is the most robust one. This is not only for the reason that the development

of the FVM is the latest in the series, but for the very reason that it adopts the same principles of the FVM that have been widely used in the analysis of fluid flow and heat transfer problems. Further, unlike the DOM [12, 13], the FVM is fully conservative. In this, the ray effect is the minimal. However, even with the FVM, radiation still remains a computationally expensive component.   Therefore, search for a computationally more efficient method still continues.

The lattice Boltzmann method (LBM) [21, 22] is a relatively new computational tool which has found widespread applications in science and engineering. This method is viewed as a potential versatile CFD tool. Since in the LBM, processes are localized, it is well suited for a parallel architecture.

In the recent past, the LBM has been applied to a large class of fluid flow and heat transfer problems [22]. Application of the LBM to solve energy equations, in particular by means of the so-called passive scalar approach [23-28], has been known for quite some time. This has essentially been the simplest approach in which the temperature is treated as a passive scalar, which is diffused and moderately advected by the flow velocity. This particular approach has been adopted to analyze several thermal problems [23-28] that involved computations of the density, velocity and temperature fields caused by convection and/or conduction heat transfer. Those studies, did not consider the effect of volumetric radiation which is an important component in high temperature applications.

Recently, Mishra and co-workers [6, 20, 29-32] have extended the application of the LBM to formulate and solve energy equations of heat transfer problems involving thermal radiation. However, in such problems, the volumetric thermal radiation was always computed using the conventional numerical radiative transfer methods such as the DOM [12, 13], the DTM [14-16], the collapsed dimension method [17] and the FVM [18-20]. The previous studies [6, 20, 29-32] have shown the superiority of the LBM over the FDM and the FVM to solve the energy equations of heat transfer problems involving thermal radiation. However, in none of the previous studies, the computation of radiative information, which is the main time consuming component, has been computed using the LBM, and thus, the usage of the LBM for the analysis of radiative transport problems has not been investigated before. Further, in the combined mode problems studied in references [6, 20, 29-32], the computational grids of the conventional radiation solvers such as the DTM [14-16], the DOM [12, 13], the FVM [18-20], etc., have always been different from the lattices of the LBM. Thus, the radiative information computed using these methods

required to be interpolated to the lattice nodes that required an additional computational step.

Having seen the success in implementation of the LBM to a wide range of fluid flow and heat transfer problems, this work aims at investigating its usage to compute radiative information in a participating medium. In the present work, the LBM formulation is developed for a 2-D rectangular geometry, and by stretching one of its dimensions, the same is tested for the 1-D planar geometry also. Heat flux and temperature distributions are computed for different values of the extinction coefficients, and they are compared against the results obtained using the FVM. A comparison of the numbers of iterations for the converged solution and the CPU times of the LBM and the FVM is also presented.

2. Formulation

Let us consider a 2-D rectangular enclosure as shown in Fig. 1. The gray and homogeneous participating medium is absorbing, emitting and scattering. The south boundary of the enclosure is at temperature T_S and it is the source of radiation in the medium. The other three boundaries are cold. All four boundaries are diffuse and gray. The medium temperature is unknown and the thermal equilibrium in the system is only by radiation.

The radiative transfer equation in any direction $\hat{s}$ is given by [10, 11]

$$\frac{dI}{ds} = \hat{s} \cdot \nabla I = -\beta I + \kappa_a I_b + \frac{\sigma_s}{4\pi} \int_{4\pi} I \, p(\Omega, \Omega') d\Omega' \tag{1}$$

where I is the intensity, s is the geometric distance in the direction $\hat{s}$, κ_a is the absorption coefficient, $I_b = \sigma T^4 / \pi$ is the blackbody intensity, β is the extinction coefficient, σ_s is the scattering coefficient and p is the scattering phase function.

If scattering is assumed isotropic $p(\Omega, \Omega') = 1$ and a radiative equilibrium condition is considered in which case in a given control volume, volumetric emission $4\pi I_b$ equals the volumetric absorption G, Eq. (1) can be written as

$$\frac{dI}{ds} = \hat{s} \cdot \nabla I = \beta \left(\frac{G}{4\pi} - I \right) \tag{2}$$

For the discrete direction having index i, Eq. (2) is written as

$$\frac{dI_i}{ds} = \hat{s} \cdot \nabla I_i = \beta \left(\frac{G}{4\pi} - I_i \right) \tag{3a}$$

where I_i is the intensity in the discrete direction i and analogously for the transient equation [11], namely

$$\frac{1}{c} \frac{\partial I_i}{\partial t} + \hat{s} \cdot \nabla I_i = \beta \left(\frac{G}{4\pi} - I_i \right) \tag{3b}$$

where c is the speed of light.

All radiative transfer methods, viz., the DTM, the DOM, the FVM, that use the ray tracing, work with a finite number of intensities. Thus, in their formulations, assumption of some kind of angular isotropy is mandatory. In the proposed LBM, we simulate radiative energy in terms of particle distribution functions (PDFs) which carry radiative energy to the neighboring lattices only in some discrete directions. Further, in line with the LBM used in the analysis of fluid flow and heat transfer problems, in analyzing a 2-D problem, a 2-D homogenous lattice is used. Radiation is always a 3-D phenomenon, and in case of a 2-D geometry, unlike a 1-D planar medium, while using the DTM, the DOM and the FVM, azimuthal symmetry can not be applied. Since for the 2-D geometry, while using the LBM, we wish to use the 2-D lattice which lies in the solution plane (x-y plane in Fig. 1a) of the 2-D geometry under consideration, we have to assume an isotropy. Further since we are constrained to be in the solution plane and have to cover all directions now confined to the solution plane, at any point, for the radiation contained in the 4π spherical space, we assume isotropy in the polar direction γ $(0 \leq \gamma \leq \pi)$ (Fig. 1b) and thus we consider angular dependence of intensity only in the azimuthal direction δ $(0 \leq \delta \leq 2\pi)$. Different types of lattices used in the present LBM for radiation are shown in Fig. 2.

For imposing the condition of isotropy in the polar direction and then in the 2-D plane, for streaming the PDFs only in the finite discrete directions, while computing the heat flux, we apply a weight to all the intensities in the discrete directions i which is spanned from 0 to 2π (Fig. 2). The same thing we do while calculating the incident radiation in which case, the weight is different from that for the calculation of heat flux.

As shown in Fig. 2, we use $\vec{e}_i$ to indicate the generic component of the lattice and $e_i = |\vec{e}_i|$ for its magnitude.

Multiplying Eq. (3b) by e_i and assuming fictitiously that $c = e_i$, we obtain the following equation

$$\frac{\partial I_i}{\partial t} + \vec{e}_i \cdot \nabla I_i = \frac{D_i I_i}{Dt} = e_i \beta \left(\frac{G}{4\pi} - I_i \right), \qquad i = 1, 2, \ldots M \tag{4}$$

where the velocity $\vec{e}_i$ propagates information along the lattice link i and M is the total number of discrete directions in the solution plane. The assumption $c = e_i$ means that the fictitious speed of light is tuned, along each discrete direction, in such a way to fit the considered computational lattice. In this way, the real transient description given by Eq. (3b) is lost, but an effective numerical tool is obtained for solving steady state problems.

Integrating Eq. (4) along the characteristic directions and keeping constant the right hand side during the discretization step (piecewise constant approximation of the integrand), the following equation is derived

$$I_i \left(\vec{r}_n + \vec{e}_i \Delta t, t + \Delta t \right) = I_i \left(\vec{r}_n, t \right) + \Delta t e_i \beta \left(\frac{G}{4\pi} - I_i \right) \tag{5}$$

In the LBM, information exchange takes place by collisions among PDFs. After collisions, they relax towards the equilibrium state and then carry the information to the neighboring lattice nodes in the directions of their propagations. From the initial condition, evolution to the steady-state takes place through multiple collisions and propagations which are highly influenced by the relaxation time. Thus, in the LBM, the relaxation time to reach the equilibrium state is an important parameter, and it tells how strong the diffusion process is.

In Eq. (5), the last term on the right hand side is the collision term and the coefficient $e_i \beta$ can be interpreted as a proper relaxation frequency for the radiation intensity along the i-th direction. Hence it is possible to introduce a relaxation time τ_i which is given by

$$\tau_i = \frac{1}{e_i \beta} \tag{6}$$

It is to be noted that the extinction coefficient β is the reciprocal of the mean free path of radiation in the medium, and $\frac{1}{\beta}$ causes a similar kind of dissipative effect to radiation as is done by momentum diffusivity (kinematic viscosity) υ in the treatment of viscous flows and thermal diffusivity α in the analysis of conduction heat transfer. The key difference here is that τ_i is a straightforward function of the transport coefficient β, which is already defined in the original physical problem given by Eq. (2), and hence there is no need to introduce any asymptotic expansion technique (e.g. Chapman-Enskog). Moreover, even though different τ_i are used for different azimuthal directions, this formulation is still

substantially based on a single-relaxation-time approach, because the differences among τ_i are due to differences among the magnitudes of the lattice velocities e_i, which are purely geometrical parameters prescribed by the considered lattice. Summarizing, the relaxation times τ_i depend on combinations of the physical parameter β and lattice-dependent geometrical parameters e_i, according to Eq. (6).

It is to be noted that in the LBM terminology, I_i is PDF and it is the carrier of the radiative energy. $\dfrac{G}{4\pi}$ is the equilibrium PDF and it can be denoted as $I^{(eq)}$. Thus, in the usual LBM formulation, Eq. (5) can be written as

$$I_i\left(\vec{r}_n + \vec{e}_i\Delta t, t + \Delta t\right) = I_i\left(\vec{r}_n, t\right) + \frac{\Delta t}{\tau_i}\left[I_i^{(eq)}\left(\vec{r}_n, t\right) - I_i\left(\vec{r}_n, t\right)\right] \tag{7}$$

In Eq. (7), the equilibrium PDF $I^{(eq)}$ is computed from the following

$$I_i^{(eq)} = \sum_{i=1}^{M} I_i \, w_{gi} \tag{8}$$

where w_{gi} is the weight corresponding to the discrete direction i. It is computed from the following

$$w_{gi} = \left(\frac{1}{4\pi}\right)\int_0^{\pi} \sin\gamma \, d\gamma \int_{\delta_i - \frac{\Delta\delta_i}{2}}^{\delta_i + \frac{\Delta\delta_i}{2}} d\delta = \frac{\Delta\delta_i}{2\pi} \tag{9}$$

It is to be noted that the angular regions of influence of all the PDFs I_i are not the same. In the D2Q8 lattice in which the 2π angular space is discretized into 8 divisions (Figs. 2 and 3a), all directions are equally spaced and hence $\Delta\delta_i$ is the same for all and it equals $\pi/8$ (Fig. 3a). In the D2Q16 lattice (Figs. 2 and 3b), while keeping the 8 directions of the D2Q8 lattice fixed, 8 more directions are added as shown in Figs. 2 and 3b. Similarly, when we move to the D2Q32 lattice, the 16 directions of the D2Q16 lattice remain intact and 16 new directions are considered as shown in Fig. 2. Therefore, unlike the D2Q8 lattice, in the D2Q16 and the D2Q32 lattices, angular spans of different PDFs are different. For any lattice, the angular span for a PDF in any direction i is determined as shown in Figs. 3a and 3b. In Fig. 3a, angular spans have been shown for PDFs in directions 1, 5 and 4. In Fig. 3b, the same have been shown for the PDFs in directions 1, 9, 5 and 10.

It is to be noted that the velocities of all PDFs I_i are not the same. For the 32 directions shown in Fig. 2, velocities are given by

$$e_{1,3} = (\pm 1, 0) \cdot U, \quad e_{2,4} = (0, \pm 1) \cdot U, \quad e_{5,6,7,8} = (\pm 1, \pm 1) \cdot U$$
$$e_{9,12} = (\pm 2, 1) \cdot U, \quad e_{13,16} = (\mp 2, -1) \cdot U$$
$$e_{10,11} = (\pm 1, 2) \cdot U, \quad e_{14,15} = (\mp 1, -2) \cdot U$$
$$e_{17,24} = (\pm 3, 1) \cdot U, \quad e_{25,32} = (\mp 3, -1) \cdot U$$
$$e_{18,23} = (\pm 3, 2) \cdot U, \quad e_{26,31} = (\mp 3, -2) \cdot U \qquad (10)$$
$$e_{19,22} = (\pm 2, 3) \cdot U, \quad e_{27,30} = (\mp 2, -3) \cdot U$$
$$e_{20,21} = (\pm 1, 3) \cdot U, \quad e_{28,29} = (\pm 1, -3) \cdot U$$

where $U = \dfrac{\Delta x}{\Delta t}$ is the speed and it has been assumed that $\Delta x = \Delta y$. It is to be noted that the directions 1-8 correspond to the D2Q8 lattices, 1-16 correspond to the D2Q16 lattice and for the D2Q32 lattices, the directions are 1-32. It is to be further noted that in the D2Q32 lattice, 5 different energy shells exist, and for directions 1, 5, 9, 17 and 18, the magnitudes of the propagation velocities are $U, U\sqrt{2}, U\sqrt{5}, U\sqrt{10}$ and $U\sqrt{13}$, respectively. In general, this means that we can express the magnitude of the lattice velocity as $e_i = \varepsilon_i U$, where ε_i is a constant depending on the energy shell of the considered velocity ($1, \sqrt{2}, \sqrt{5}, \sqrt{10}, \sqrt{13}$ in the previous examples).

The radiative heat fluxes along x- and y-faces of the 2-D rectangular enclosure (Fig. 1) are computed from the following

$$q_x = \sum_{i=1}^{M} I_i w_{xi}, \quad q_y = \sum_{i=1}^{M} I_i w_{yi} \qquad (11)$$

where the weights w_{xi} and w_{yi} are given by

$$w_{xi} = \int_0^{\pi} \sin^2 \gamma \, d\gamma \int_{\delta_i - \frac{\Delta \delta_i}{2}}^{\delta_i + \frac{\Delta \delta_i}{2}} \cos \delta \, d\delta = \pi \cos \delta_i \sin\left(\frac{\Delta \delta_i}{2}\right) \qquad (12a)$$

$$w_{yi} = \int_0^{\pi} \sin^2 \gamma \, d\gamma \int_{\delta_i - \frac{\Delta \delta_i}{2}}^{\delta_i + \frac{\Delta \delta_i}{2}} \sin \delta \, d\delta = \pi \sin \delta_i \sin\left(\frac{\Delta \delta_i}{2}\right) \qquad (12b)$$

The incoming unknown PDFs are computed from the knowledge of the temperature of the boundary and for a black boundary, the same are given by

$$I_i = \frac{\sigma T_w^4}{\pi} \qquad (13)$$

Eqs. (6) – (8) combined with Eq. (11) describe the evolution of the PDFs on the lattice. From the view point of the solution procedure, the algorithm can be split into two steps, viz., collision and streaming, and they are given by Eqs. (14a) and (14b), respectively.

$$I_i^* (\vec{r}_n, t) = I_i (\vec{r}_n, t) + \frac{\Delta t}{\tau_i} \left[I_i^{(eq)} (\vec{r}_n, t) - I_i (\vec{r}_n, t) \right] \tag{14a}$$

$$I_i (\vec{r}_n + \vec{e}_i \Delta t, t + \Delta t) = I_i^* (\vec{r}_n, t) \tag{14b}$$

3. Results and Discussion

3.1 Error Analysis

Before reporting the performance of the proposed approach in solving some test cases, a general error analysis for the LBM scheme is discussed. Essentially the error analysis aims to investigate the dependence of the numerical error of the proposed scheme with regards to the main discretization parameters, namely mesh size and adopted lattice.

Let us combine Eq. (4) and Eq. (6), namely

$$\frac{\partial \bar{I}_i}{\partial t} + \vec{e}_i \cdot \nabla \bar{I}_i = \frac{1}{\tau_i} \left(\bar{I}_i^{(eq)} - \bar{I}_i \right) \tag{15}$$

where the bar above the radiation intensity means the ideal solution of the radiation problem and the equilibrium radiation intensity can be computed (ideally) as

$$\bar{I}_i^{(eq)} = \left(\frac{1}{4\pi} \right) \int_0^{2\pi} \int_0^{\pi} \bar{I} \sin \gamma \, d\gamma \, d\delta = \left(\frac{1}{4\pi} \right) \sum_{i=1}^{M} \int_{\delta_i - \frac{\Delta\delta_i}{2}}^{\delta_i + \frac{\Delta\delta_i}{2}} \int_0^{\pi} \bar{I} \sin \gamma \, d\gamma \, d\delta \tag{16}$$

The previous integral is still exact. Taylor expanding the generic argument $\bar{I}(\delta, \gamma)$ around the term $\bar{I}_i(\delta_i, \frac{\pi}{2})$ aligned with the considered lattice yields

$$\bar{I}(\delta, \gamma) = \bar{I}_i(\delta_i, \frac{\pi}{2}) + \frac{\partial \bar{I}}{\partial \delta}\bigg|_i (\delta - \delta_i) + \frac{\partial \bar{I}}{\partial \gamma}\bigg|_i (\gamma - \frac{\pi}{2}) + O\left((\delta - \delta_i)^2 \right) + O\left((\gamma - \frac{\pi}{2})^2 \right) \tag{17}$$

where $O(\cdot)$ indicates the magnitude order of a function according to the Landau notation. Substituting the previous expansion into Eq. (16) yields

$$\bar{I}_i^{(eq)} = \sum_{i=1}^{M} \bar{I}_i \, w_{gi} + O(\max_{1 \leq i \leq M}(\Delta\delta_i)) + E_\gamma \tag{18}$$

where E_γ is a constant due to the fact that the polar angle is not actually discretized. The first term at the right hand side of the previous equation is exactly the quadrature reported in Eq. (8). However the error analysis applied to the equilibrium term given by Eq. (16) reveals that the previous quadrature is first order with regards to the subdivision $\Delta\delta_i$ of the azimuthal angle considered by the lattice and it implies a fixed error with regards to the polar discretization (as expected). This means that, since the proposed approach lies on the

computational plane, it cannot improve the numerical solution with regards to the polar angle dependence. The practical magnitude of the fixed term E_γ must be evaluated according to the considered application.

Proceeding in a similar way with the left hand side of Eq. (15) and taking into account Eq. (18) yield

$$\frac{\bar{I}_i(\vec{r}_n + \vec{e}_i\,\Delta t, t + \Delta t) - \bar{I}_i(\vec{r}_n, t)}{\Delta t} = \frac{1}{\tau_i}\left(\sum_{i=1}^{M}\bar{I}_i\,w_{gi} - \bar{I}_i\right) + O\big((1+\varepsilon_i)\,\Delta x\big) + O(\max_{1\le i\le M}(\Delta\delta_i)) + E_\gamma \qquad (19)$$

where $e_i = \varepsilon_i\,U$ and $U = \dfrac{\Delta x}{\Delta t}$ is assumed constant (due to stability constraints). The left hand side and the first term on the right hand side represent exactly the proposed numerical scheme given by Eqs. (7, 8, 9). Hence the error analysis allows one to prove that

$$E_{tot} = O\big((1+\varepsilon_i)\,\Delta x\big) + O(\max_{1\le i\le M}(\Delta\delta_i)) + E_\gamma \qquad (20)$$

Few considerations immediately follow. It is evident from the previous expression that the dependence of the global error on the discretization parameters is not trivial. In fact, improving the discretization of the azimuthal angle, i.e. reducing $\max_{1\le i\le M}(\Delta\delta_i)$, forces one to consider larger lattices, with larger energy shells, which usually spoil the accuracy of the advection step (because of larger ε_i). On the other hand, accurate advection step requires a compact computational stencil, i.e. few energy shells, but this makes quite rough the discretization of the azimuthal angle and consequently the computation of the collision step (by the definition of local equilibrium). With other words, because of the geometrical construction, the following relation holds $\varepsilon_i \propto 1/\max_{1\le i\le M}(\Delta\delta_i)$. Hence there is a trade off between the accuracy of the advection step and that of the collision step, which both affect the global error.

Secondly, in order to recover the minimum error, i.e. E_γ, the azimuthal discretization must be chosen accordingly to the mesh discretization, i.e. $\Delta\delta_i \propto \Delta x$. This may be sometimes unpractical, because it would require increasing the number of the lattice velocities when refining the spatial mesh. However even though it is unpractical, it represents the right framework for validation purposes.

Thirdly, the integration along the characteristics by keeping fixed the right hand side of Eq. (4), leading to Eq. (5), requires that $\Delta t\,\beta = \Delta x\,\beta / U$ is small enough to achieve a stable

solution with acceptable accuracy. Hence it is possible to define a radiation Knudsen number as

$$Kn = \Delta x \, \beta \qquad\qquad (21)$$

In the following simulations, the spatial discretization has been chosen in such a way that the Knudsen number is smaller than a threshold value that ensures stability and accuracy of the solution, namely $Kn = \Delta x \, \beta \leq 0.05$.

3.2 2-D Rectangular Enclosure

In the following pages, we validate the present LBM formulation. For the purpose of validation, results of the standard FVM are considered benchmark [11]. In particular, the FVM code of the second co-author (SCM), which has been used for various problems, was used in the present work for generating the FVM results. Both the LBM and the FVM are iterative methods. The LBM on one hand solves even a steady-state problem in a transient mode with an imposed initial condition. The FVM proceeds to solve the same by starting from a guess value, and as the number of iterations proceeds, the solution approaches convergence. Thus, both the LBM and the FVM require a convergence criterion on one of the evolving parameters. In the present work, this was set on the incident radiation, and when between the two successive iterations, the maximum change in incident radiation at any point was less than 1×10^{-6}, the solution was assumed to have converged.

First of all, a grid convergence analysis has been performed. The reference numerical solutions are obtained by Richardson extrapolation of FVM results. In particular, spatial meshes of 80×80 and 160×160 nodes are used for extrapolating the reference solution for the extinction coefficient $\beta = 2.0$, while meshes of 200×200 and 400×400 nodes are used for the extinction coefficient $\beta = 5.0$. In all cases, the following stability criterion holds $Kn = \Delta x \, \beta \leq 0.05$. The azimuthal angle is discretized by 32 subdivisions and the polar angle by 16 subdivisions.

Once the reference solution is obtained, the validation analysis has been performed focusing on the dimensionless heat flux $\Psi_y = \dfrac{q_y}{\sigma T_S^4}$. The numerical results for LBM are reported in Table 1: in particular, the dimensionless total heat flux along the south wall (Table 1a); the mean temperature of the medium inside the enclosure (Table 1b) and the errors of the dimensionless heat flux with regards to discretizations and extinction

coefficients (Table 1c). The LBM results were obtained by spatial meshes of 40×40, 80×80, 160×160 nodes and 100×100, 200×200, 400×400 nodes for $\beta = 2$ and $\beta = 5$ respectively. For each case, three azimuthal discretizations were used, namely $M = 8, 16, 32$. It is clear from the results of Table 1, that the LBM results reached good grid convergence (or equivalently mesh independence).

Let us introduce the following global error

$$ E_{LBM} = \frac{\left\| \Psi_{LBM} - \Psi_{FVM,0} \right\|_2}{\left\| \Psi_{FVM,0} \right\|_2} \tag{22} $$

where $\Psi_{FVM,0}$ is the reference solution for the dimensionless heat flux obtained by the FVM and Ψ_{LBM} is the generic LBM solution. The numerical values for this error are reported in Table 1c. It is clear that there is error saturation because of the residual term E_γ (see Eq. (20)) due to the extremely poor polar discretization (all the intensities lie on the computational plane for $\gamma = \frac{\pi}{2}$). Hence the results reported in Table 1c show that improving further the azimuthal and the space discretization is not rewarding for the present test case because, beyond some point, the global error depends mainly by the assumption on the polar angle discretization. However extending the present approach for more complex discretizations of the polar angle is not difficult. It is enough to prescribe that the projections of the discrete velocities on the computational domain belong to the considered lattice.

After discussing the error analysis and showing the grid convergence, more simulations were run for investigating the practical advantages of the proposed scheme. For these additional simulations, in case $\beta \leq 5.0$, both the LBM and the FVM runs were taken for 31×31 lattice/control volumes. For a higher value of the extinction coefficient $\beta > 5.0$, in the LBM runs were taken for 101×101 lattices.

In Figs. 4a-4c, distributions of the dimensionless heat flux $\Psi = \frac{q}{\sigma T_s^4}$ along the south (hot) boundary have been compared between the LBM and the FVM. In Fig. 4a, these comparisons are made for the extinction coefficient $\beta = 1.0, 3.0$ and 5.0. Fig. 4b shows this comparison for $\beta = 10.0$ and 15.0. For $\beta = 20.0$ and 30.0, the same are shown in Fig. 4c. The FVM results have been obtained for 8×16 directions and the LBM results have been

computed for the D2Q16 lattice which uses only 16 directions. It is seen from Figs. 4a – 4c that for all values of the extinction coefficient β, results of the LBM follow the trend and also compare closely with those of the FVM.

The comparison of the LBM and the FVM results for the centreline $\left(\dfrac{x}{X} = 0.5, y \right)$ dimensionless emissive power $\Phi = \left(\dfrac{T}{T_S} \right)^4$ has been shown in Figs. 5a -5f. In Fig. 5a, results have been compared for $\beta = 1.0$ and 3.0. In Fig. 5b – 5f, the same has been done for $\beta = 5.0, 10.0, 15.0, 20.0$ and 30.0, respectively. It is seen from Fig. 5a that for $\beta = 1.0$, the emissive power distribution has a numerical oscillation. This oscillation is present in both the FVM and in the LBM. However, it is more prominent in the LBM. By increasing the number of control volumes, this unphysical numerical oscillation can be avoided. For higher values of the extinction coefficient β, the emissive power computed using the LBM is found to match well with those of the FVM.

Discretization error is inherent with every numerical method. In both the LBM and the FVM, the angular distributions of intensity spanned over 4π spherical space are discretized into some finite number of directions. In the FVM, the discrete intensities are spanned over the 2π spherical space, while in the LBM formulation used in the present work, as shown in Fig. 2, they exit in the solution plane of the 2-D enclosure and they span over the circular space of 4π which is the span of the azimuthal angle δ. As mentioned previously, in the LBM formulation, isotropy was assumed in the polar direction.

In Figs. 6a-6c, we compare the effect of lattices in the LBM and the number of directions in the FVM on the dimensionless heat flux Ψ distributions along the south (hot) boundary. In Figs. 6a-6c, comparisons have been made for the extinction coefficient $\beta = 1.0, 5.0$ and 10.0, respectively. For the LBM, effects of D2Q8, D2Q16 and D2Q32 have been studied, while, for the FVM, effects have been studied for 2×4, 4×8 and 8×16 azimuthal directions. It is obvious from these figures that both in the LBM and the FVM, results improve by increasing the number of directions.

In the LBM formulation, from D2Q16 to D2Q32, not much improvement is observed. In the FVM, this trend was observed when the number of directions was increased beyond 8×16.

3.3 1-D Planar Medium

Having validated the proposed 2-D LBM formulation, we next see how it performs for the case of a 1-D planar medium. For this case, the X-dimension in the 2-D LBM code was stretched 10 times more than the Y-dimension, i.e, $\dfrac{X}{Y}$ was set to 10. With this, practically the effects of the side walls (west and east) should have no influence on the heat flux at the center $\left(\dfrac{x}{X}=0.5, \dfrac{y}{Y}=0.0\right)$ of the south wall and emissive power distributions along the centerline $\left(\dfrac{x}{X}=0.5, \dfrac{y}{Y}\right)$. This particular situation corresponds to the 1-D planar medium. To compare the LBM results for this case, the 1-D FVM code especially meant for the 1-D planar medium was used in which the south boundary was made hot and the north boundary was made cold. In Figs. 7a and 7b, results of the LBM and the FVM are compared.

Fig. 7a provides a comparison of the variation of the dimensionless heat flux Ψ on the hot (south) boundary with the extinction coefficient β. This comparison has been made for the extinction coefficient values $\beta \in \{0.1, 0.5, 1, 2, 3, 4, 5, 6, 7, 8, 9, 10\}$. The LBM results show a good comparison with the FVM results.

The dimensionless emissive power Φ distributions in the medium have been compared in Fig. 7b for $\beta = 1.0, 3.0, 5.0$ and 10.0. With an increase in the value of β, results of the two methods are found to compare well.

The LBM as such is an established method for the analysis of fluid flow and heat transfer problems. However, the present work is the first work that deals with its application to compute radiative information, which in combined mode problems remains a computationally expensive task. Methods such as the DTM, the DOM and the FVM for computations of radiative information are well established and they have been widely used in the combined mode problems. Apart from extending the LBM formulation to a pure radiative transport problem, one of the main objectives of the present work has been to explore its computational efficiency of the LBM and compare the same with its FVM counterpart which is a widely used method. Figures 8 and 9 present results on number of iterations and the CPU time used in the LBM. Figures 8a and 8b show variations in the number of iterations for extinction coefficient β in the range $\beta \in \{1, 5, 10, 15, 20, 25\}$ for the

LBM and the FVM, respectively. Figure 8c compares variations of the CPU time (s) with β for the LBM and the FVM. For results in Figs. 8a-8c, in both the LBM and the FVM, 51×51 control volumes/lattices were used. In the FVM, 8×16 discrete directions were used, while the D2Q32 lattice was used in the LBM. All computations were performed on two Xeon Quad Core Processors, 2.66 GHz, 8 GB SDRAM RDIMM.

It is seen from Figs. 8a and 8b that compared to the FVM, the number of iterations for the converged solution in the LBM is much higher. It is three orders of magnitude higher than that for the FVM. However, as seen from Fig. 8c, the CPU time of the LBM is found much lower than that of the FVM. With increase in β, the LBM is found to be computationally more efficient. This implies that although the LBM takes much iteration, per iteration it spends much less time than that of the FVM. This is an attractive feature of the LBM for radiation. This computational efficiency of the LBM is attributed to the fact that even with the D2Q32 lattice, the LBM uses ¼ times less number of directions than that of the FVM which has used 8×16 directions. As in the combined mode problems, the computation of radiative information remains the most expensive aspect, with the usage of the LBM, a drastic saving of computational time will result.

In combined mode problems like the natural convection in a cavity [32], with increase in Rayleigh number, the requirement of computational nodes/lattices increases drastically. With volumetric radiation, the computational time becomes exorbitant. Keeping this fact in mind, how the number of iterations and CPU change with increase in the number of lattices in the LBM, the results are presented in Figs. 9a and 9b. These results are presented for extinction coefficient $\beta=1.0, 5.0$ and 10.0. The number of lattices has been varied from 11×11 to 401×401. It is seen from Fig. 9a that the number of iterations increases with increase in β and for a higher value of β, this increase is more. An interesting feature is observed from Fig. 9b. Even with 401×401 lattices for $\beta=10.0$ when the number of iterations is 289 millions, the LBM takes only about 13 minutes time to provide the converged solution. Thus, like the LBM widely used in fluid flow and heat transfer problems, the proposed LBM in this work has a great potential for its use in the combined mode problems involving thermal radiation.

4. Conclusions

The usage of the LBM was extended to solve radiative transport problems in an absorbing, emitting and scattering medium. A 2-D formulation of the LBM was developed for the analysis of radiative transport problems. The formulation was tested for radiative equilibrium problems. A benchmark radiative transport problem in a 2-D square enclosure was considered. To compare the results of the LBM, the problem was also solved using the FVM. The FVM results were considered benchmark after applying the Richardson extrapolation. Dimensionless heat flux distributions along the hot boundary and centreline emissive power distributions were compared for a wide range of values of the extinction coefficient. By stretching x-dimension of the 2-D enclosure, a 1-D planar medium situation was achieved and results for this case were compared with the 1-D FVM code. For all the situations, the LBM results were in good agreements with the FVM results, with the exception of small boundary effects. The number of iterations and the CPU times in the LBM and the FVM were also compared. The LBM was found to take more iterations than the FVM. However, computationally the LBM was much more efficient than the FVM. By increasing the number of lattices in the LBM, the number of iterations was found to increase drastically, but the CPU time as still found much lower.

The present work being the first on implementation of the LBM to radiative transport problems, a further careful look is needed to study the methodology to improve its accuracy and to test it for other types of problems, especially the combined mode problems which are computationally very expensive. Work in this direction is underway.

References

1. J. G. Marakis, C. Papapavlou, and Kakaras, E., A Parametric Study of Radiative Heat Transfer in Pulverised Coal Furnaces, *Int. J. Heat Mass Transfer*, vol. 43, pp. 2961-2971, 2000.
2. M. Spinnler, E. R. F. Winter, and R. Viskanta, Studies on High-Temperature Multilayer Thermal Insulations, *Int. J. Heat Mass Transfer*, vol. 47, pp. 1305-1312, 2004.

3. C. Yao, G.X. Wang, and B.T.F. Chung, Nonequilibrium Planar Interface Model for Solidification of Semitransparent Radiating Materials. *J. Thermophys Heat Transfer*, vol. 14, pp. 297-304, 2000.

4. Y. Shu, B.Q. Al, L. A1, and K.G. Lynn, Numerical Modeling of Internal Radiation and Solidification in Semitransparent Melts in Magnetic Fields, *Numer. Heat Transfer B*, vol. 45, pp. 957-976, 2004.

5. P. Sadooghi, Transient Coupled Radiative and Conductive Heat Transfer in a Semitransparent Layer of Ceramic, *J. Quant. Spectros. Radiat. Transfer*, vol. 92, pp. 403-416, 2005.

6. R. Raj, A. Prasad, P.R. Parida, and S.C. Mishra, Analysis of Solidification of a Semitransparent Planar Layer using the Lattice Boltzmann Method and the Discrete Transfer Method, *Numer. Heat Transfer A*, vol. 49, pp. 279-299, 2006,

7. W. W. Grabowski, Impact of Cloud Microphysics on Convective—Radiative Quasi Equilibrium Revealed by Cloud-resolving Convection Parameterization, *J. Clim.* vol. 16, pp. 3463–3475, 2003.

8. K. Kim and Z. Guo, Ultrafast Radiation Heat Transfer in Laser Tissue Welding and Soldering, *Numer. Heat Transfer A*, vol. 46, pp.23-40, 2004.

9. G. Pal, S. Basu, K. Mitra, and S. Kumar, Bioheat Transfer in Layered Skin Model Subjected to Short Pulse Laser Irradiation, *Laser Surg. Med.,* vol. 13, pp. 12-37, 2005.

10. R. Siegel and J. R. Howell, *Thermal Radiation Heat Transfer*, fourth ed., Taylor & Francis, New York, 2002.

11. M.F. Modest, *Radiative Heat Transfer*, second ed., Academic Press, New York, 2003.

12. W.A. Fiveland, Discrete-Ordinates Solution of the Radiative Transport Equation for Rectangular Enclosures, *J. Heat Transfer*, vol. 106, pp. 699–706, 1984.

13. S.C. Mishra, H.K. Roy, and N. Misra, Discrete Ordinate Method with a New and a Simple Quadrature Scheme, *J. Quant. Spectrosc. Radiat. Transfer*, vol. 101, pp. 249-262, 2006.

14. F.C. Lockwood, and N.G. Shah, A New Radiation Solution Method for Incorporation in General Combustion Prediction Procedures. In: Eighteenth Symposium (Int.) on Combustion, The Combustion Institute, Pittsburgh, pp. 1405–1414, 1981.

15. P.S. Cumber and M. Fairweather, Evaluation of Flame Emission Models Combined with the Discrete Transfer Method for Combustion System Simulation, *Int. J. Heat Mass Transfer*, vol. 48, pp. 5221-5239. 2005.

16. N. Anand and S.C. Mishra, The Discrete Transfer Method Applied to the Radiative Heat Transfer in a Variable Refractive Index Semitransparent Medium, *J. Quant. Spectrosc. Radiat. Transfer*, vol. 102, pp. 432-440, 2006.

17. S.C. Mishra and M. Prasad, Radiative Heat Transfer in Absorbing-Emitting-Scattering Gray Media Inside 1-D Gray Cartesian Enclosure using the Collapsed Dimension Method, *Int. J. Heat Mass Transfer*, vol. 45, pp. 697-700. 2002.

18. J.C. Chai and S.V. Patankar, Finite Volume Method for Radiation Heat Transfer, *Adv. Numerical Heat Transfer*, vol. 2, pp. 110–135, 2000.

19. M.Y. Kim, S.W. Baek, and C.Y. Lee, Prediction of Radiative Heat Transfer Between Two Concentric Spherical Enclosures with the Finite Volume Method. *Int. J. Heat Mass Transfer*, vol. 51, pp. 4820-4828, 2008.

20. S.C. Mishra and H.K. Roy, Solving Transient Conduction-Radiation Problems using the Lattice Boltzmann Method and the Finite Volume Method, *J. Comput. Physics*, vol. 223, pp. 89-107, 2007.

21. S. Chen and G.D. Doolen, Lattice Boltzamann Method for Fluid Flows, *Annu. Rev. Fluid Mech.*, vol. 30, pp. 329-364. 1998.

22. S. Succi, *The Lattice Boltzmann Method for Fluid Dynamics and Beyond*, Oxford University Press, New York, 2001.

23. F. Massaioli, R. Benzi, and S. Succi, Exponential Tails in Rayleigh-Benard Convection, *Europhys. Lett.,* vol. 21, pp. 305-310, 1993.

24. J.G.M. Eggels and J.A. Sommers, Numerical Simulation of Free Convective Flow using the Lattice-Boltzmann Scheme, *Int. J. Heat Fluid Flow*, vol. 16, pp. 357-364, 1995.

25. X. Shan, Simulation of Rayleigh-Bénard Convection using a Lattice Boltzmann Method, *Phys. Rev. E*, vol. 55, pp. 2780-2788, 1997.

26. S. Succi, G. Bella, and F. Papetti, Lattice Kinetic Theory for Numerical Combustion, *J. Sci. Comput.* vol. 12, pp. 395-408, 1997.

27. X. He, S. Chen, and G.D. Doolen, A Novel Thermal Model for the Lattice Boltzmann Method in Incompressible Limit, *J. of Comp. Physics*, vol. 146, pp. 282-300, 1998.

28. R.G.M. van der Sman, M.H. Ernst, and A.C. Berkenbosch, Lattice Boltzmann Scheme for Cooling of Packed Cut Flowers, *Int. J. Heat Mass Transfer*, vol. 43, pp. 577-587, 2000.

29. S.C. Mishra, A. Lankadasu, and K. Beronov, Application of the Lattice Boltzmann Method for Solving the Energy Equation of a 2-D Transient Conduction-Radiation Problem, *Int. J. Heat Mass Transfer*, vol. 48, pp. 3648-3659. 2005.

30. R. Das, S.C. Mishra, M. Ajith, and R. Uppaluri, An Inverse Analysis of a Transient 2-D Conduction-Radiation Problem Using the Lattice Boltzmann Method and the Finite Volume Method Coupled with the Genetic algorithm. *J. Quant. Spectrosc. Radiat. Transfer*, vol. 109, pp. 2060-2077, 2008.

31. S.C. Mishra, T.B. Pavan Kumar, and B. Mondal, Lattice Boltzmann Method Applied to the Solution of Energy Equation of a Radiation and Non-Fourier Heat Conduction Problem, *Numer. Heat Transfer A*, vol. 54, pp. 798-818, 2008.

32. B. Mondal, and S.C. Mishra, Simulation of Natural Convection in the Presence of Volumetric Radiation Using the Lattice Boltzmann Method, *Numer. Heat Transfer A*, vol. 55, pp. 18-41, 2009.

List of Figures

Figure 1: (a) 2-D rectangular geometry and the computational grid under consideration, (b) the coordinate system used.

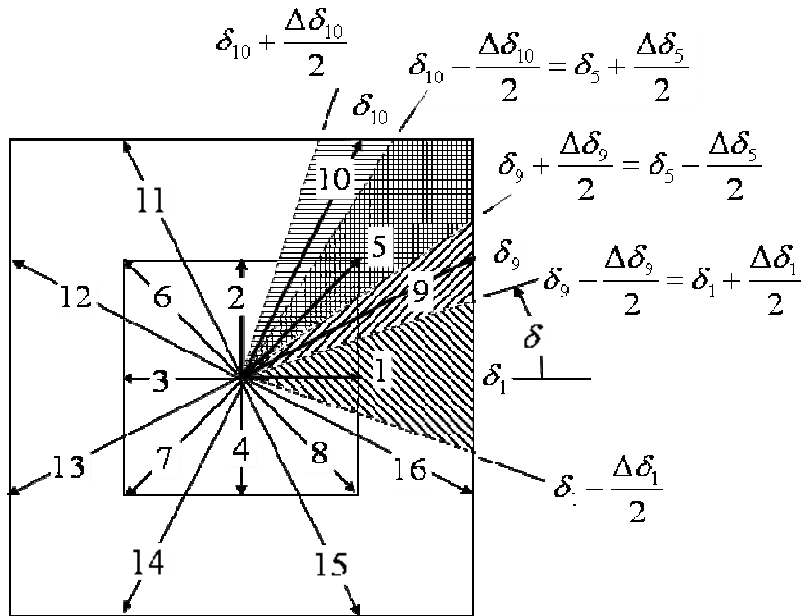**Figure 2:** Schematic of the lattices D2Q8: 1-8, D2Q16: 1-16 and D2Q32: 1-32 directions.

Figure 3: Schematic of the region of influence of the particle distribution functions in the directions (a) 1, 5 and 4 in the D2Q8 lattice and (b) 1, 9, 5 and 10 in the D2Q16 lattice.
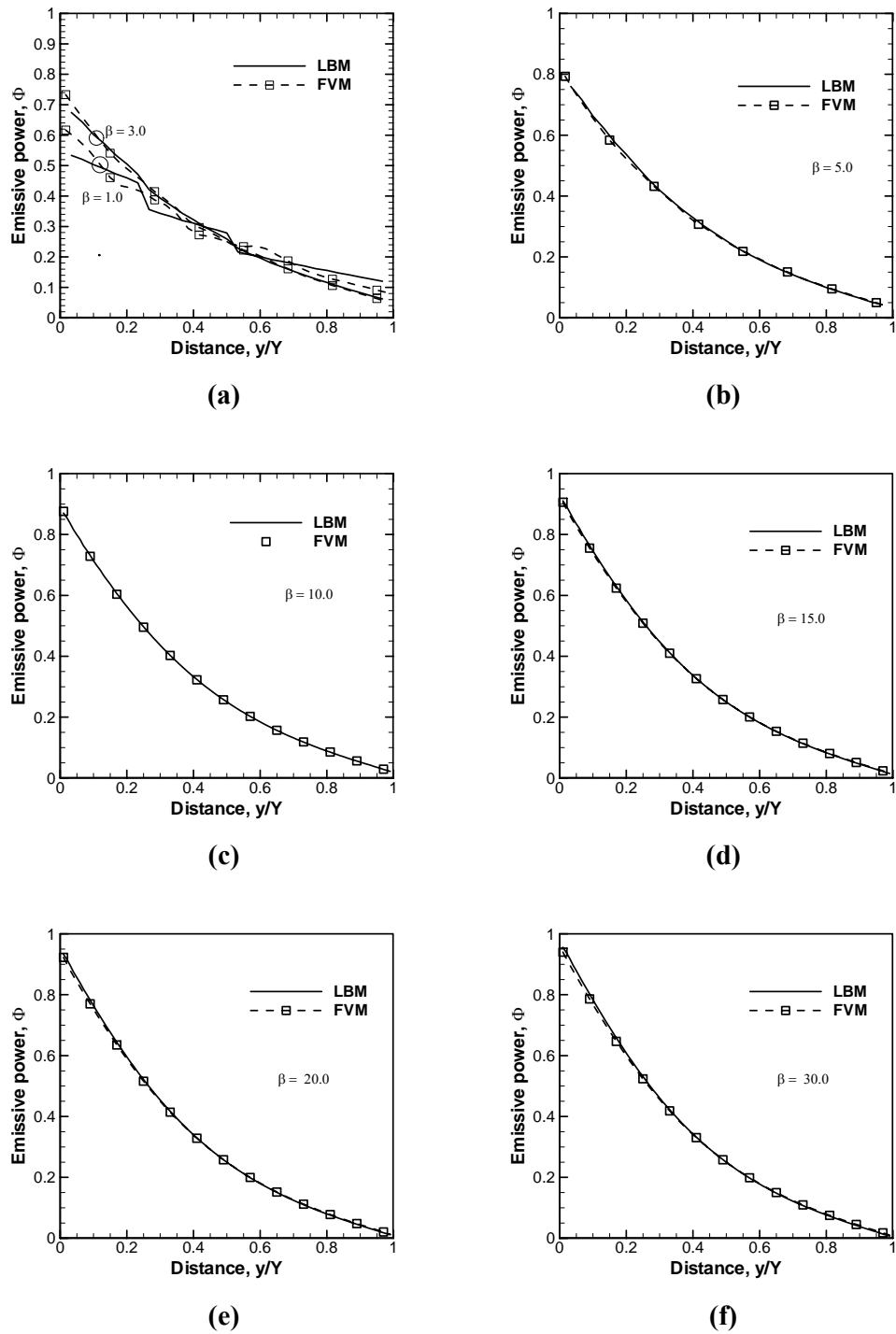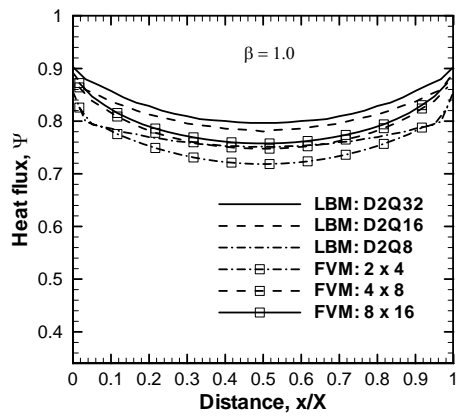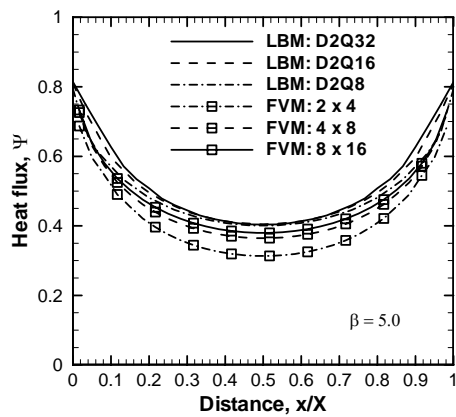
Figure 4: Comparison of dimensionless heat flux Ψ distribution along the south wall for extinction coefficient (a) $\beta = 1.0, 3.0$ and 5.0 and (b) $\beta = 10.0$ and 15 and (c) $\beta = 20.0$ and 30.0.
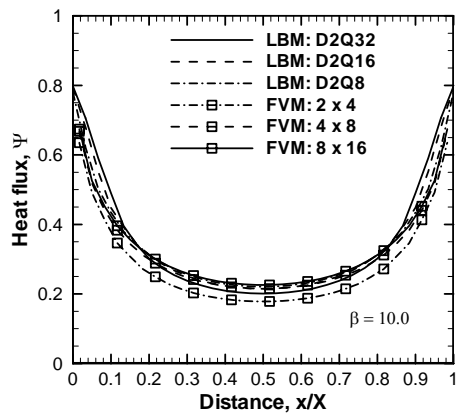
Figure 5: Comparison of dimensionless centreline emissive power Φ distribution for extinction coefficient (a) $\beta = 1.0$ and 3.0, (b) $\beta = 5.0$, (c) $\beta = 10.0$, (d) $\beta = 15.0$, () $\beta = 20.0$ and (f) $\beta = 30.0$.
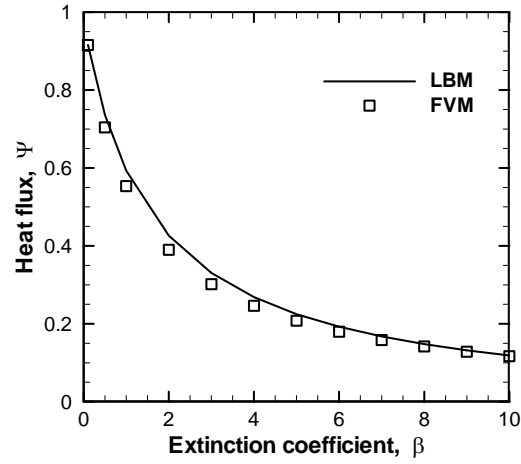
Figure 6: Comparison of dimensionless heat flux Ψ distribution along the south wall for D2Q8, D2Q16 and D2Q32 lattices for extinction coefficient (a) $\beta = 1.0$, $\beta = 5.0$ and $\beta = 10.0$.

Figure 7: Comparison of (a) variations of dimensionless heat flux Ψ on the south boundary with the extinction coefficient β and (b) distributions of dimensionless emissive power Φ in the medium for $\beta = 1.0, 3.0, 5.0$ and 10.0.

Figure 8: Change in number of iterations with a change in the extinction coefficient β in (a) LBM and (b) FVM and (c) comparison of CPU times in the LBM and the FVM.

Figure 9: Variation of the (a) number of iterations with the number of lattices and (b) the CPU time with the number of lattices in the LBM for extinction coefficient $\beta = 1.0, 5.0$ and 10.0.
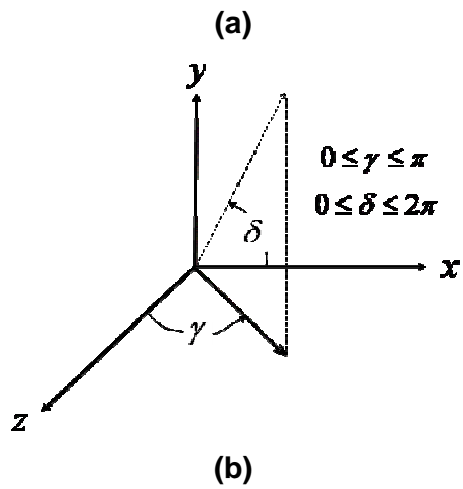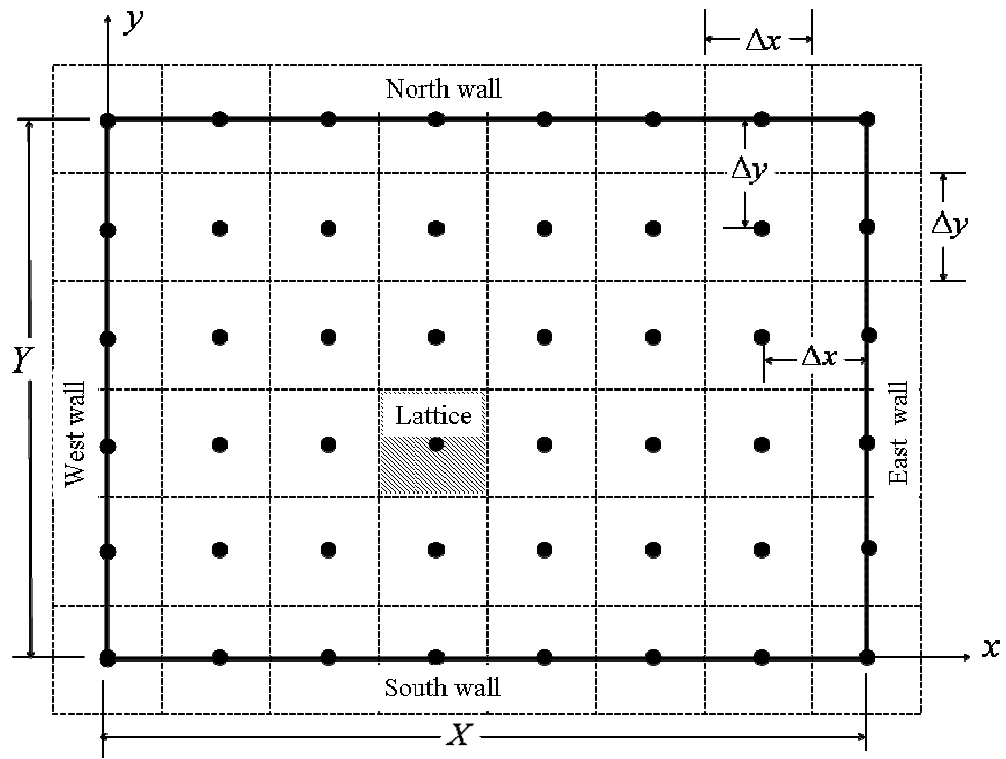
Figure 1: **(a)** 2-D rectangular geometry and the computational grid under consideration, (b) the coordinate system used.
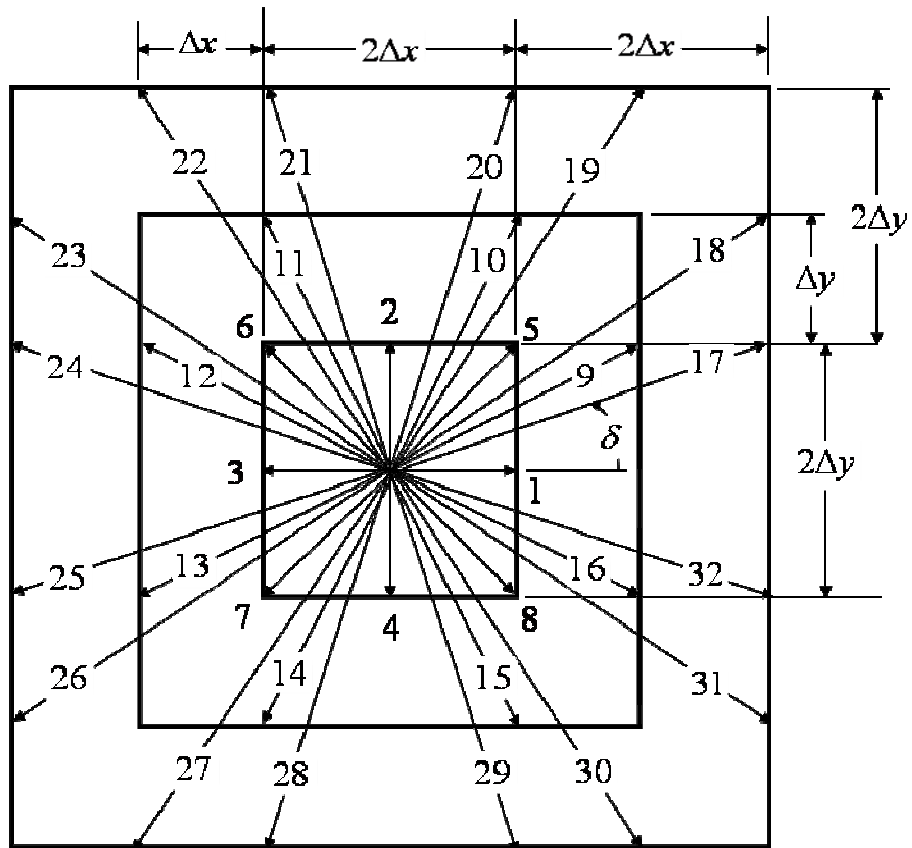
Figure 2: Schematic of the lattices   D2Q8: 1-8, D2Q16: 1-16 and D2Q32: 1-32 directions.
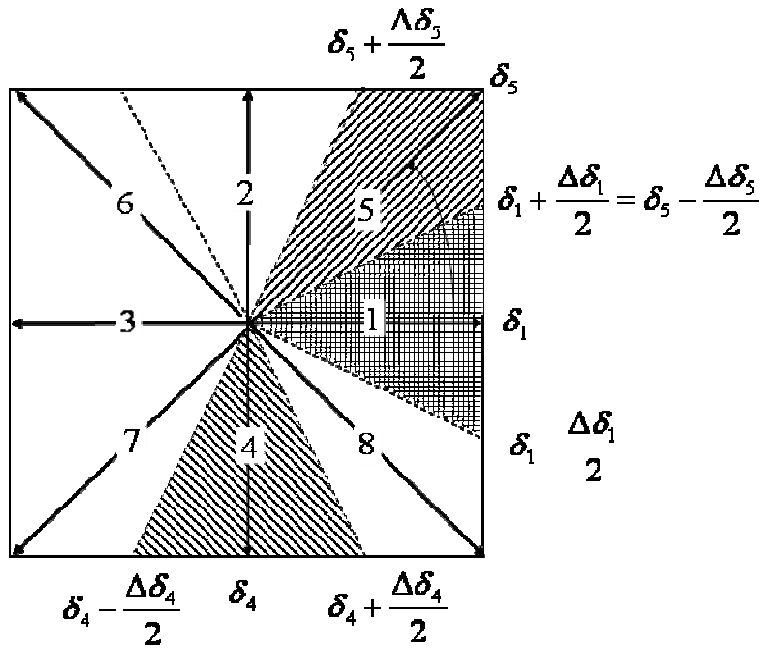
(a)

(b)

Figure 3: Schematic of the region of influence of the particle distribution functions in the directions (a) 1, 5 and 4 in the D2Q8 lattice and (b) 1, 9, 5 and 10 in the D2Q16 lattice.
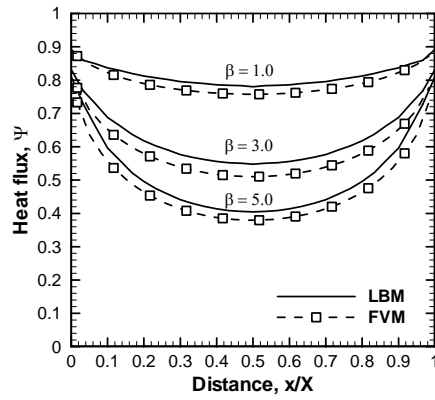
(a)
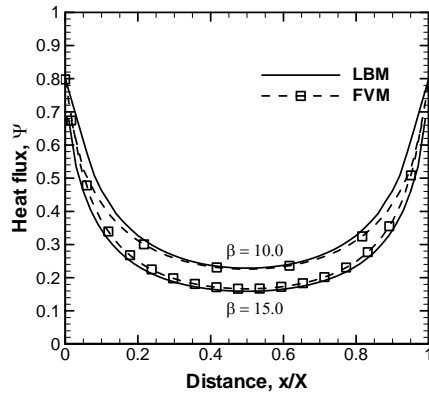
(b)
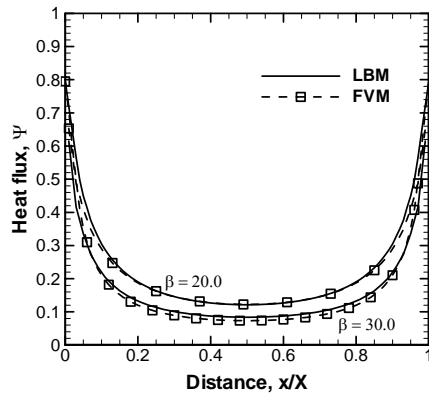
(c)

Figure 4: Comparison of dimensionless heat flux Ψ distribution along the south wall for extinction coefficient (a) $\beta = 1.0, 3.0$ and 5.0 and (b) $\beta = 10.0$ and 15 and (c) $\beta = 20.0$ and 30.

Figure 5: Comparison of dimensionless centreline emissive power Φ distribution for extinction coefficient (a) $\beta = 1.0$ and 3.0, (b) $\beta = 5.0$, (c) $\beta = 10.0$, (d) $\beta = 15.0$, (e) $\beta = 20.0$ and (f) $\beta = 30.0$.

(a)

(b)

(c)

Figure 6: Comparison of dimensionless heat flux Ψ distribution along the south wall for D2Q8, D2Q16 and D2Q32 lattices for extinction coefficient (a) $\beta = 1.0$, (b) $\beta = 5.0$ and (c) $\beta = 10.0$.
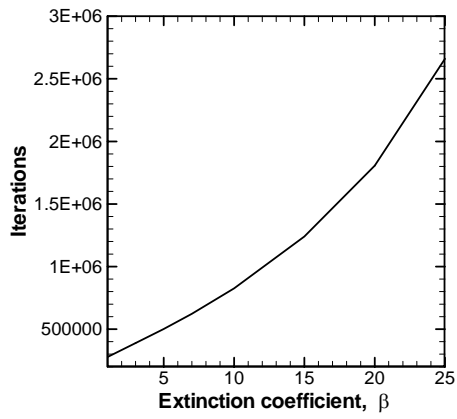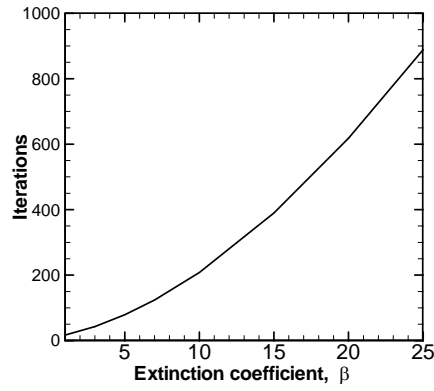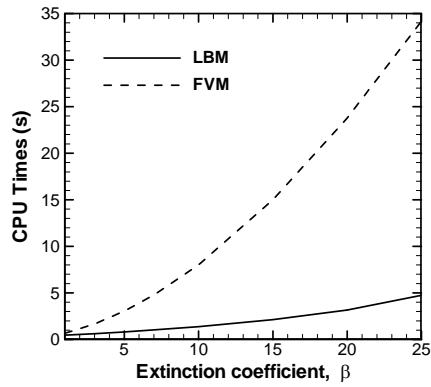

(a)
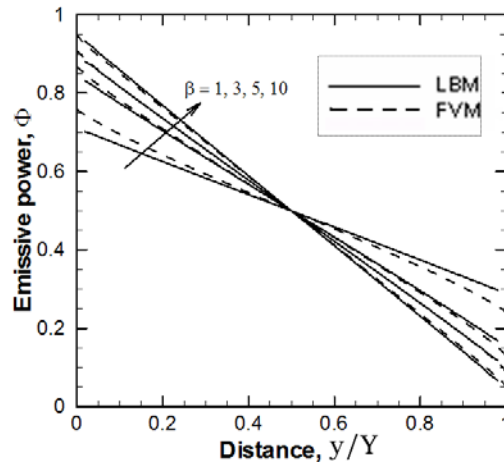
(b)

Figure 7: Comparison of (a) variations of dimensionless heat flux Ψ on the south boundary with the extinction coefficient β and (b) distributions of dimensionless emissive power Φ in the medium for $\beta = 1.0, 3.0, 5.0$ and 10.0.
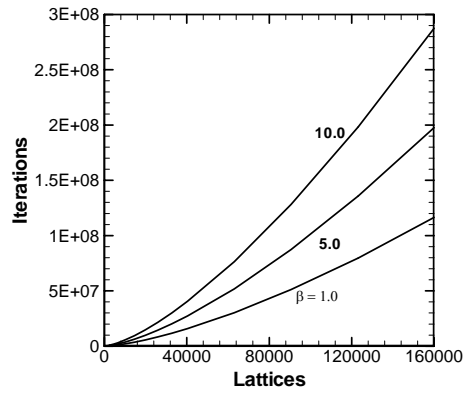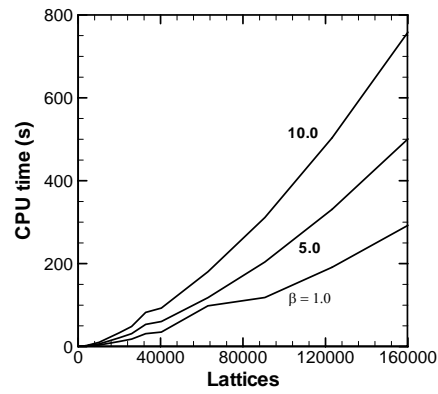
(a)

(b)

(c)

Figure 8: Change in number of iterations with a change in the extinction coefficient β in (a) LBM and (b) FVM and (c) comparison of CPU times in the LBM and the FVM.

(a)

(b)

Figure 9: Variation of the (a) number of iterations with the number of lattices and (b) the CPU time with the number of lattices in the LBM for extinction coefficient $\beta = 1.0, 5.0$ and 10.0.

List of Tables

Table 1: Comparison between LBM and FVM results for the 2-D rectangular enclosure: (a) dimensionless total heat flux along the south wall; (b) mean temperature of the medium inside the enclosure; (c) errors of the dimensionless heat flux with regards to discretizations and extinction coefficients.

(a)

	β = 2.0			β = 5.0		
	$N_x = 40$	$N_x = 80$	$N_x = 160$	$N_x = 100$	$N_x = 200$	$N_x = 400$
M = 8	0.67840	0.67316	0.67050	0.49908	0.49733	0.49645
M = 16	0.71062	0.70430	0.70117	0.51616	0.51431	0.51338
M = 32	0.72273	0.71421	0.71020	0.52166	0.51925	0.51808

(b)

	β = 2.0			β = 5.0		
	$N_x = 40$	$N_x = 80$	$N_x = 160$	$N_x = 100$	$N_x = 200$	$N_x = 400$
M = 8	0.63122	0.65742	0.67072	0.64538	0.65593	0.66123
M = 16	0.62911	0.65528	0.66855	0.64364	0.65427	0.65962
M = 32	0.62785	0.65440	0.66787	0.64298	0.65387	0.65935

(c)

	β = 2.0			β = 5.0		
	$N_x = 40$	$N_x = 80$	$N_x = 160$	$N_x = 100$	$N_x = 200$	$N_x = 400$
M = 8	*0.14875*	0.13922	0.13618	*0.13572*	0.12638	0.12264
M = 16	0.13591	*0.11843*	0.11129	0.14796	*0.13389*	0.12757
M = 32	0.14174	0.11801	*0.10759*	0.15775	0.13937	*0.13092*